# Chapter 2

# Out-of-time-order correlation and detection of phase structure in Floquet transverse Ising spin system

## 2.1 Introduction

In the last two decades, out-of-time-order correlation (OTOC) has gained a lot of attention among researchers in various fields. One field of interest is the butterfly effects in quantum chaotic systems [8, 13, 14, 15]. Other directions are quantum information scrambling [14, 18, 39, 91, 92, 93, 94, 95, 96] and many-body localization [97]. The nontrivial OTOC as a holographic tool has been instrumental in determining the interplay of scrambling, and entanglement [98, 99]. Many experiments have been done to measure OTOCs in various systems , *e.g.*, trapped-ion quantum magnets [100], and nuclear magnetic resonance quantum simulator [101].

In addition to the above fields of interest, the OTOCs are useful in determining phases of the quantum critical systems [50, 102, 103]. The phase structures of quantum critical systems have been studied extensively in the last few decades [102, 103, 104, 105, 106,

107, 108, 109, 110, 111, 112, 113, 114, 115]. One of the simplest models to display and analyze the quantum phase transition is one dimensional transverse Ising model, which Hamiltonian is given as $H = J\sum_i \sigma_i^x \sigma_{i+1}^x + h\sum_i \sigma_i^z$. This system undergoes a phase transition at $J = h$ from the ferromagnetic state ($J > h$) to the paramagnetic phase ($J < h$) [49, 50, 51, 52]. Such phase transitions in time-independent equilibrium systems have been well-studied over the years. In the last few years, the OTOC has emerged as a tool to detect equilibrium and dynamical quantum phase transitions in the transverse field Ising (TFI) model and the Lipkin-Meshkov-Glick model (LMG) [50].

It has been shown that the OTOC of the ground states and quenched states can diagnose the quantum phase transitions and dynamical phase transition, respectively [50]. The ferromagnetic ($J > h$)and paramagnetic ($J < h$) phases of the transverse Ising model can be characterized by nonzero and zero long-time averaged OTOC, respectively[50]. Periodically driven quantum systems, known as the Floquet systems, which have properties of the duality between time and space [116] and time-reflection symmetry [117], on the other hand, pose a different problem: one would expect generic Floquet systems to heat to infinite temperatures. However, specific cases of nonergodic phases with localization have been observed in Floquet systems [118, 119]. In these systems, multiple nonergodic phases with differing forms of dynamics and ordering have been observed [114]. These multiple phases are characterized by broken symmetries and topological order. In the case of transverse Ising Floquet systems, Majorana modes are produced at the ends of the chain [107]. The zero-energy Majorana mode corresponds to the long-range ferromagnetic order, while the nonzero-energy Majorana mode corresponds to the paramagnetic phase [106, 107]. The sharp phase boundaries of the Floquet Ising system are explained by symmetry-protected Ising order [109, 114]. For binary Floquet drive, two paramagnetic and two ferromagnetic phases can be seen in the phase diagram. The two paramagnetic/ferromagnetic phases are distinguished by the combined eigenvalues

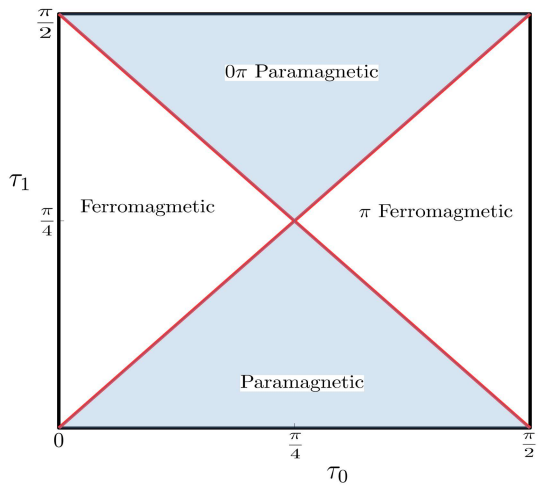


Fig. 2.1 Phase structure of the Floquet system with Floquet map given by Eq. (2.1). There are four distinct phases in the $\tau_0 - \tau_1$ parameter space. Two of these phases, the $\pi$ ferromagnetic and the $0\pi$ paramagnetic, are phases which are unique to Floquet systems.

at the edges of the Floquet drives and the parity operators. On the basis of the combined eigenvalues, the paramagnetic region is divided into two parts: 0 and $0\pi$-paramagnetic, and ferromagnetic region is also divided into two parts: 0 and $\pi$-ferromagnetic [Fig. 2.1]. In the ferromagnetic region, all eigenstates have long-range Ising symmetry broken order. However, in the paramagnetic phase, all eigenstates have long-range symmetric order.

First, we will consider transverse magnetization out-of-time-order correlation (TMOTOC) and calculate the exact solution using the Jordan Wigner transformation by mapping the spin operators onto the fermionic annihilation and creation operators. Next, we will consider the longitudinal magnetization out-of-time-order correlation (LMOTOC) and explore the various phases in the Fouquet Ising spin system.

In this chapter, we will start discussing the model of the Floquet system. Subsequently, we will define the longitudinal and transverse magnetization OTOCs. We will introduce the time average of the LMOTOC for the detection of phase structures and discuss the various phases of the Floquet Ising system using a long-time averaged LMOTOC. Later, we conclude the results.

## 2.2 Model

We consider an integrable Floquet transverse Ising system with binary Floquet drives. The Floquet map corresponding to this system is

$$U = e^{-iH_{xx}\tau_1} e^{-iH_z\tau_0}, \tag{2.1}$$

where $H_{xx}$ is the nearest neighbor Ising interaction given by $H_{xx} = \sum_{l=1}^{N-1} \sigma_l^x \sigma_{l+1}^x$ for open chain system and $H_{xx} = \sum_{l=1}^{N} \sigma_l^x \sigma_{l+1}^x$ for closed chain system with $\sigma_{N+1}^x = \sigma_1^x$. $H_z = \sum_{l=1}^{N} \sigma_l^z$ is the transverse field in z-direction. $\tau_0$ and $\tau_1$ are the time periods. The Hamiltonian corresponding to the above Floquet operator is:

$$H(t) = H_{xx} + \sum_{n=-\infty}^{\infty} \delta\Big(n - \frac{t}{\tau_1}\Big)\frac{\tau_0}{\tau_1} H_z. \tag{2.2}$$

## 2.3 Out-of-time-order Correlation

The out-of-time order correlation (OTOC) is, in general, defined as $F(t) = \langle \hat{W}(t)\hat{V}\hat{W}(t)\hat{V}\rangle$, where $\hat{V}$ and $\hat{W}$ are two local Hermitian operators and $\hat{W}(t)$ is the Heisenberg evolution of the operator $\hat{W}$ by time $t$. We consider two different OTOCs defined as follows:

i) *Transverse magnetization OTOC (TMOTOC)* : Here we consider two local spin operators $\hat{W}$ and $\hat{V}$ in the direction perpendicular to the Ising axis (x-axis). In our generic treatment, we set the operators $\hat{W} = \hat{\sigma}_l^z$ and $\hat{V} = \hat{\sigma}_m^z$ at different sites $l$ and $m$. The TMOTOC in our protocol is given as:

$$F_z^{l,m}(n) = \langle \phi_0 | \hat{\sigma}_l^z(n)\hat{\sigma}_m^z\hat{\sigma}_l^z(n)\hat{\sigma}_m^z | \phi_0\rangle, \tag{2.3}$$

with the initial state as $|\phi_0\rangle = |\uparrow\uparrow\uparrow\cdots\uparrow\rangle$, where $|\uparrow\rangle$ is the eigenstate of $\hat{\sigma}^z$ with eigenvalue $+1$.

ii) *Longitudinal magnetization OTOC (LMOTOC)* : In this case, two local spin operators are chosen along the Ising axis, *i.e.* $\hat{W} = \hat{\sigma}_l^x$ and $\hat{V} = \hat{\sigma}_m^x$. The LMOTOC is given as follows:

$$F_x^{l,m}(n) = \langle \psi_0 | \hat{\sigma}_l^x(n) \hat{\sigma}_m^x \hat{\sigma}_l^x(n) \hat{\sigma}_m^x | \psi_0 \rangle. \tag{2.4}$$

Here $|\psi_0\rangle = |\rightarrow\rightarrow\rightarrow\cdots\rightarrow\rangle$ is the initial state with, $|\rightarrow\rangle$ is the eigenstate of $\hat{\sigma}^x$ with eigenvalue $+1$.

In what follows, $l$ and $m$ can take any value between 1 to $N$ (even) in a closed chain system. For the open chain case, we will consider the special case with $l = m = \frac{N}{2}$. The time evolution of the spin operator at the position $l$ after $n$ kicks is defined as $\hat{\sigma}_l^{z/x}(n) = \hat{U}^{\dagger n} \hat{\sigma}_l^{z/x} \hat{U}^n$. The case $l = m$ will be treated as a special case.

## 2.4 Analytical calculation of TMOTOC

Considering $t_0 = 2\tau_0$, $t_1 = 4\tau_1$ and $\hat{\sigma}_l^x = 2\hat{S}_l^x$ and periodic boundary condition in the unitary operator defined in Eq. (2.1), we get Floquet map as:

$$\hat{U} = \exp\Big[-it_1 \sum_{l=1}^{N} \hat{S}_l^x \hat{S}_{l+1}^x\Big] \exp\Big[-it_0 \sum_{l=1}^{N} \hat{S}_l^z\Big], \tag{2.5}$$

We calculate the analytical expression for the TMOTOC using the Jorden-Wigner transformation (for detailed calculation, refer to the Appendix A-I):

$$\begin{aligned} F_z^{l,m}(n) &= 1 - \Big(\frac{2}{N}\Big)^3 \sum_{p,q,r} \Big[ e^{i(p-q)(m-l)} |\Psi_r(n)|^2 \Phi_p^*(n) \Phi_q(n) \\ &- e^{i(-r-q)(m-l)} \Psi_r(n)^* \Phi_p^*(n) \Phi_q(n) \Psi_{-p}(n) \\ &- e^{i(p+q)(m-l)} \Psi_q(n) \Psi_r(n)^* \Phi_p(n)^* \Phi_{-r}(n) \\ &+ e^{i(q-r)(m-l)} \Psi_q(n) \Psi_r(n)^* |\Phi_p(n)|^2 \Big]. \end{aligned} \tag{2.6}$$

Now, we take a special case in which both the local operators are at the same position i.e. $l = m$ and $\hat{V} = \hat{W} = \hat{\sigma}_l^z$. The expression of TMOTOC simplifies to

$$\begin{aligned} F_z^{l,l}(n) &= 1 - \left(\frac{2}{N}\right)^3 \sum_{p,q,r} \Big[ |\Psi_r(n)|^2 \Phi_p(n)^* \Phi_q(n) - \Psi_{-p}(n) \Psi_r(n)^* \Phi_p(n)^* \Phi_q(n) \\ &\quad - \Psi_q(n) \Psi_r(n)^* \Phi_p(n)^* \Phi_{-r}(n) + \Psi_q(n) \Psi_r(n)^* |\Phi_p(n)|^2 \Big], \end{aligned} \tag{2.7}$$

where the expansion coefficients $\Phi_q(n)$ and $\Psi_q(n)$ are defined as

$$\begin{aligned} \Phi_q(n) &= |\alpha_+(q)|^2 e^{-in\gamma_q} + |\alpha_-(q)|^2 e^{in\gamma_q}, \\ \Psi_q(n) &= \alpha_+(q)\beta_+(q) e^{-in\gamma_q} + \alpha_-(q)\beta_-(q) e^{in\gamma_q}. \end{aligned} \tag{2.8}$$

The phase angle $\gamma_q$ and the coefficients $\alpha_\pm(q)$ and $\beta_\pm(q)$ are given by

$$\cos(\gamma_q) = \cos(t_0)\cos(t_1) - \cos(q)\sin(t_0)\sin\left(\frac{t_1}{2}\right), \tag{2.9}$$

and

$$\alpha_\pm(q)^{-1} = \sqrt{1 + \left(\frac{\cos(\frac{t_1}{2}) - cos(\gamma_q \pm t_0)}{\sin(q)\sin(t_0)\sin(\frac{t_1}{2})}\right)^2}, \tag{2.10}$$

$$\beta_\pm(q) = \frac{\mp \sin(\gamma_q) - \cos(t_0)\cos(q)\sin(\frac{t_1}{2}) - \sin(t_0)\cos(\frac{t_1}{2})}{\sin(q)\sin(\frac{t_1}{2})} \alpha_\pm e^{-it_0}(q). \tag{2.11}$$

The allowed value of $p$, $q$ and $r$ are from $\frac{-(N-1)\pi}{N}$ to $\frac{(N-1)\pi}{N}$ differing by $\frac{2\pi}{N}$ for even number of $N_F$ ($N_F = c_l^\dagger c_l$, number of fermions).

The values of $F_z^{l,l}(n)$ obtained by the analytical expression in Eq. (2.7) exactly match with those obtained by numerical exact diagonalization as shown in Fig. 2.2.

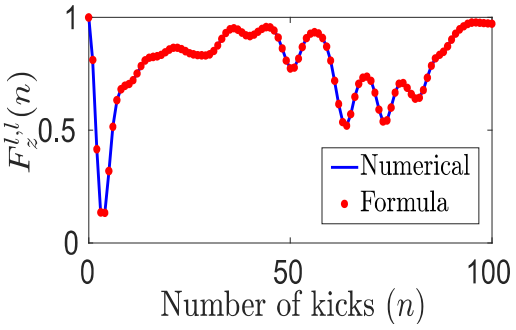


Fig. 2.2 $F_z^{l,l}(n)$ for closed chain transverse Ising Floquet system of system size $N = 12$ by using the numerical calculations (solid line) and analytical expression of Eq. (2.7) (point). Here we take $\tau_0 = \tau_1 = \varepsilon$, where $\varepsilon = \frac{\pi}{28}$.

## 2.5 Speed for correlation propagation

Next, we use Eq. (2.6) for $l \neq m$ to calculate the speed for correlation propagation. At $t = 0$, both the operators $\hat{W}(t = 0) = \hat{\sigma}_l^z$ and $\hat{V} = \hat{\sigma}_m^z$, commute with each other which implies that $F_z^{l,m}(n)$ will be unity. As time changes, the evolution of $\hat{\sigma}_l^z$ takes place by the Floquet operator; they no longer commute. Therefore, $F_z^{l,m}(n)$ starts to drop from the unity, which provides us the speed of correlation propagation ($v_{cp}$). The general approach to calculate $v_{cp}$ is as follows: First, we fix $m = \frac{N}{2}$ and change $l$ from $\frac{N}{2}+1$ to $\frac{N}{2}+5$. By using Fig. 2.3(a), we determine the characteristic time $t_{\Delta l}$ in which $F_z^{l,m}(n)$ starts departing from unity and plot it as a function of the separation between the observables ($\Delta l$) [inset of Fig. 2.3(a)]. In the inset of Fig. 2.3(a), dots are the points corresponding to the given $\Delta l$ and dashed line is the best fit line. Reciprocal of the slope of this straight line is the speed of the correlation propagation $v_{cp}$. For comparison, we have shown similar results for LMOTOC in Fig. 2.3(b). We find that the speed of the commutator growth of the $F_z^{l,m}(n)$ ($v_{cp} = 0.175$) is nearly equal to that of the $F_x^{l,m}(n)$ ($v_{cp} = 0.181$). This means that $v_{cp}$ is independent of the choice of the observables. By comparing Fig. 2.3(a) and (b), we observe that the closer the operators $\hat{V}$ and $\hat{W}$ are, the smaller the characteristic time $t_{\Delta l}$ is.

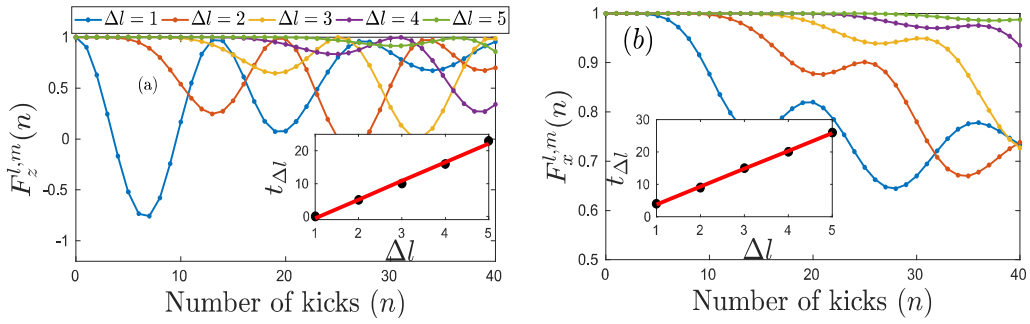


Fig. 2.3 Behaviour of (a) $F_z^{l,m}(n)$ and (b)$F_x^{l,m}(n)$ with number of kicks for different value of $\Delta l$. Here, the parameters are: $\tau_0 = \frac{\varepsilon}{2}$, $\tau_1 = \varepsilon$, and $N = 12$. In both figures (a) and (b), the inset shows the behavior of time of departure from unity ($t_{\Delta l}$) as a function of separation between the observables ($\Delta l$)

.

## 2.6 Revival time

Now we move to another interesting quantity, the revival time of $F_z^{l,m}(n)$ and $F_x^{l,m}(n)$, which is defined as the time in which OTOCs return back to their initial value. We can see from Fig. 2.3(a,b) that the early time behavior of both $F_z^{l,m}(n)$ and $F_x^{l,m}(n)$ looks very similar. For instance, both $F_z^{l,m}(n)$ and $F_x^{l,m}(n)$ start deviating from unity after a certain time. However, the long time behaviors of $F_z^{l,m}(n)$ and $F_x^{l,m}(n)$ differ widely. After decreasing from unity to a minimum, $F_z^{l,m}(n)$ revives and recovers to its initial value, *i.e.,* unity, while $F_x^{l,m}(n)$ oscillates about a finite value and never reaches to unity. Revival time depends on the distance between local operators. The larger the separation between the operators $\hat{V}$ and $\hat{W}$ is, the more the revival time is. This can be seen from Fig. 2.3(a,b).

The advantage of having an easily computable formula such as Eq. (2.7) is that we can study the TMOTOC as a function of Floquet periods $\tau_0$ and $\tau_1$ and see the behavior at any number of kicks. The analytical expression is of $O(L^3)$, which has a significant advantage over exact diagonalization calculations of $O(2^L)$ [inset of Fig. 2.4(a)].

The LMOTOCs have been shown to be useful in detecting the phase transitions between the paramagnetic and ferromagnetic phases in spin systems [50]. However, the same cannot

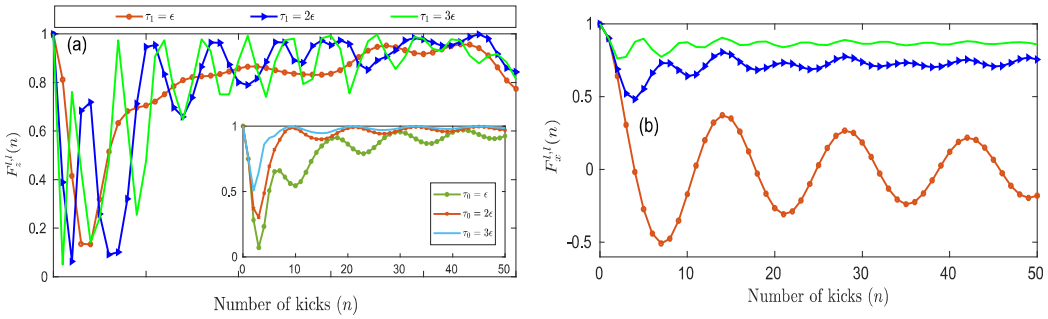


Fig. 2.4 (a) Variation of the real part of (a) $F_x^{l,l}(n)$ and (b) $F_x^{l,l}(n)$ with number of Floquet periods for a fixed $\tau_0 = \varepsilon$ and $\tau_1 = \varepsilon$, $2\varepsilon$ and $3\varepsilon$ in closed chain Floquet systems with system size N=12. Inset of the figure is the variation of $F_z^{l,l}(n)$ with the number of Floquet periods for a fixed $\tau_1 = \frac{\pi}{24}$ and $\tau_0 = \varepsilon$, $2\varepsilon$ and $3\varepsilon$ in closed chain Floquet systems with system size N=50.

be said about TMOTOC using the same concept. A comparison of the behavior of the two quantities with time is shown in Fig. 2.4. We see from Fig. 2.4(a) that TMOTOCs always oscillate about a positive value for all the pairs of $\tau_0$ and $\tau_1$, signaling that the long time average of TMOTOC is always a positive quantity. However, in the case of LMOTOCs, as shown in 2.4(b), we find that the long-time average value can be either zero or a positive quantity. In order to detect the phase structure of the system, we require the order parameter characterizing the distinct phases to show a sharp contrast between the phases. We see that the LMOTOCs qualify the criterion to be used as an order parameter, but TMOTOCs fail to do so.

Upon performing a quantum quench from a polarized state, we will use the saturation value of the LMOTOC as the order parameter to distinguish between the two phases. It is calculated by numerical methods because a compact analytical expression is not achievable using the Jordan-Wigner transformation. A possible approach and inability to get a compact analytical solution for LMOTOC is given in the Appendix (A-II).

We study the phase structure of the system [Eq. (2.1)] by calculating the LMOTOC [Eq. (2.4)]. If LMOTOC saturates to a particular value after a long period of time, this value can be determined by taking the long-time average of the LMOTOC. We define the

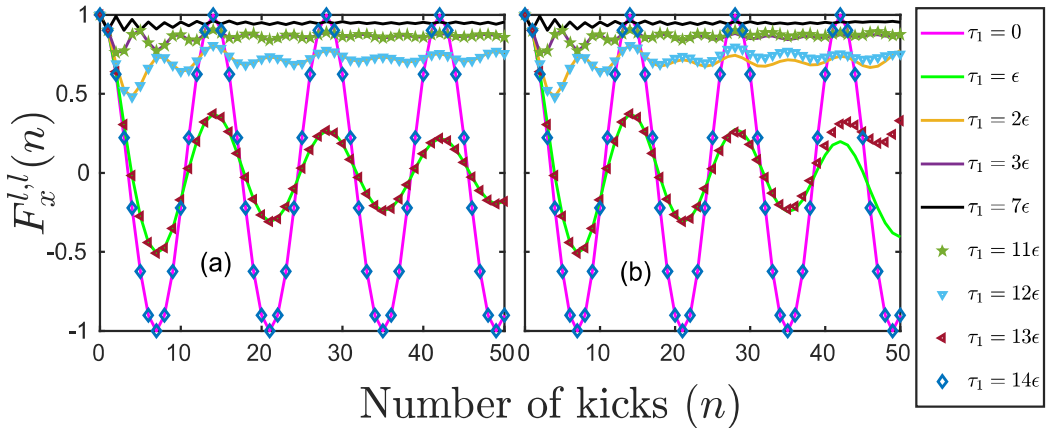


Fig. 2.5 Variation of the real part of $F_x^{l,l}(n)$) with the number of Floquet periods for a fixed $\tau_0 = \varepsilon = \frac{\pi}{28}$ and multiple values of $\tau_1$ in (a) closed and (b) open chain Floquet systems with system size N=12. The initial state is a direct product of the eigenstate of $\sigma^x$ with eigenvalue $+1$. At $\tau_1 = 0$, $F_x^{l,l}(n)$ shows periodic oscillations about zero. As the value of $\tau_1$ is increased, the $F_x^{l,l}(n)$ oscillates about greater non-zero values with lower amplitudes of oscillation and at $\tau_1 = \frac{\pi}{4}$, it saturates to the value 1. As increase constant value of $\tau_1$, $F_x^{l,l}(n)$ has same and different value as $\frac{\pi}{2} - \tau_1$ in closed and open chain respectively.

long time average of the LMOTOC, $\overline{F}_x^{l,l}(T)$ upto $T$ Floquet periods by:

$$\overline{F}_x^{l,l} = \frac{1}{T}\sum_{n=1}^{T} F_x^{l,l}(n). \tag{2.12}$$

The long-time average of the LMOTOC has a direct link with the spectral properties of the system in consideration [120]. The averaged LMOTOC links with the spectral form factor [121], a well-known quantity in random matrix theory, which is a quantifier for discreteness in the spectrum.

## 2.7 Phase Structure

The phase structure of the Floquet system given by Eq. (2.1) is known to have four distinct phases in the two-dimensional parameter space of $\tau_0$ and $\tau_1$. The phase diagram is shown in Fig. 2.1 [106, 109, 114]. Paramagnetic and ferromagnetic phases show behavior similar

to their undriven counterparts. The other two of the phases observed, the $\pi$-ferromagnetic and $0\pi$-paramagnetic, are unique to Floquet systems and are not observed in undriven non-Floquet systems. The phase transitions between these phases in the $\tau_0$ and $\tau_1$ parameter space can be detected by calculating LMOTOCs. The LMOTOC has been shown to saturate to non-zero values in the ferromagnetic region and zero in the paramagnetic region at long times in the undriven systems [50]. Hence, the long-time averaged LMOTOC serves as a good order parameter for paramagnetic and ferromagnetic regions in the undriven systems. In driven Floquet systems, LMOTOCs do not saturate to non-zero and zero values for all values of $\tau_0$ and $\tau_1$; we see a continuing oscillating behavior about a non-zero or zero mean value (Fig. 2.5). The time-averaged LMOTOC ($\overline{F}_x^{l,l}(n)$) is seen to saturate at long times in the thermodynamic limit to non-zero values in the ferromagnetic and $\pi$ ferromagnetic regions and zero in the paramagnetic and $0\pi$ paramagnetic regions of the phase space. Fig. 2.6 shows the variation of the long time-average of the real part of the LMOTOC with $\tau_1$, for different values of $\tau_0$ in the closed and open boundary conditions for a system size $N = 10$.

The critical points where the phase transition occurs are identified along the constant $\tau_0$ line at the points where LMOTOC goes from zero to non-zero. These critical points, when mapped in the $\tau_0$ and $\tau_1$ parameter space for $N = 6, 8$ and 10, give plots as shown in Fig. 2.7.

There exists a symmetry along $\tau_1 = \frac{\pi}{4}$ in the closed chain case because the behavior of LMOTOC is the same for Floquet period $\tau_1$ and $\frac{\pi}{2} - \tau_1$ (*e.g.,* $\varepsilon$ and $13\varepsilon$, $2\varepsilon$ and $12\varepsilon$, $3\varepsilon$ and $11\varepsilon$ are same in Fig. 2.5(a)). In the open chain case, LMOTOC for long-time is different for $\tau_1$ and $\frac{\pi}{2} - \tau_1$ (see, for example, $\varepsilon$ and $13\varepsilon$, $2\varepsilon$ and $12\varepsilon$, $3\varepsilon$ and $11\varepsilon$ in Fig. 2.5(b)), therefore the symmetry along $\tau_1 = \frac{\pi}{4}$ is absent in Fig. 2.7(b). However, a symmetry along $\tau_0 = \frac{\pi}{4}$ exists in both open and closed chain [Fig. 2.7(a,b)]. We demonstrate these symmetries for the closed chain system using a toy model of two and four spins. First,

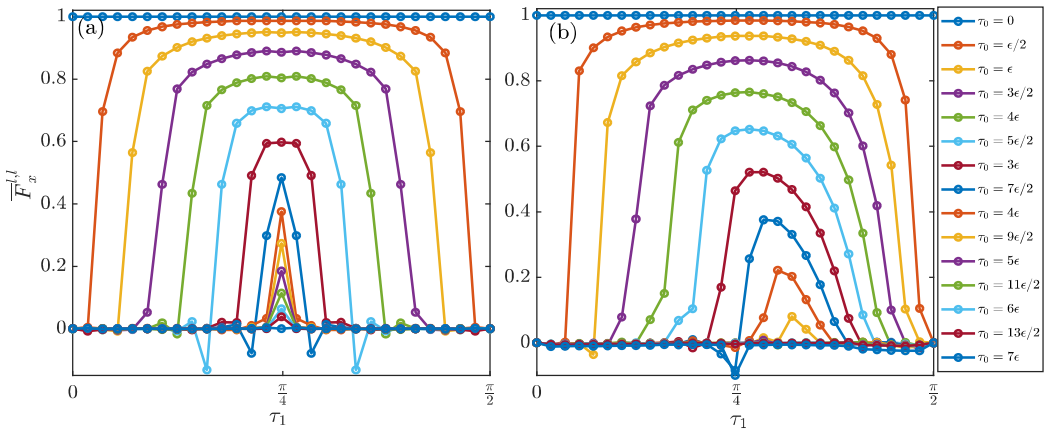


Fig. 2.6 Plot of $\overline{F}_x^{l,l}(T)$ with $\tau_1$ for values of $\tau_0$ varying from 0 to $\frac{\pi}{4}$ in intervals of $\epsilon$ in the (a) closed and (b) open chain Floquet systems of system size $N = 10$ and $T = 10^4$. The variation of $\overline{F}_x^{l,l}(T)$ with $\tau_1$ for $\pi/4 < \tau_0 < \pi/2$ is the same as that for $\frac{\pi}{2} - \tau_0$. This plot can be used to find the regions in the $\tau_0$ and $\tau_1$ parameter space that have $\overline{F}_x^{l,l}(T) > 0$ and $\overline{F}_x^{l,l}(T) = 0$ (Fig. 2.7).

we calculate $F_x^{l,l}(n)$ for two spin system: After the first kick ($n = 1$), $F_x^{l,l}(1) = \cos(4\tau_0)$. Since the magnetization is in the direction of coupling of spins, the interaction term $H_{xx}$ (with $\tau_1$) is not involved in the state after the first kick. After the second kick ($n = 2$) LMOTOC is given by

$$\begin{aligned} F_x^{l,l}(2) &= \frac{1}{8}\Big[1 - 4\cos(4\tau_1) - 4\cos(4\tau_0)\Big(-1 + \cos(8\tau_1)\Big) \\ &+ 3\cos(8\tau_1) + \cos(8\tau_0)\Big(3 + 4\cos(4\tau_1) + \cos(8\tau_1)\Big)\Big]. \end{aligned}$$

The symmetry along $\tau_0 = \pi/4$ is evident in the above expression as $\tau_0$, and $\tau_1$ appear in the expression with a multiple of $4k$, where $k$ is an integer. Further kicking the system will also manifest the multiplicity of $4k$ with $\tau_0$ and $\tau_1$. Next, we take the toy model of four spins case. LMOTOC after the first kick ($n = 1$) will again be $F_x^{l,l}(1) = \cos(4\tau_0)$ and after

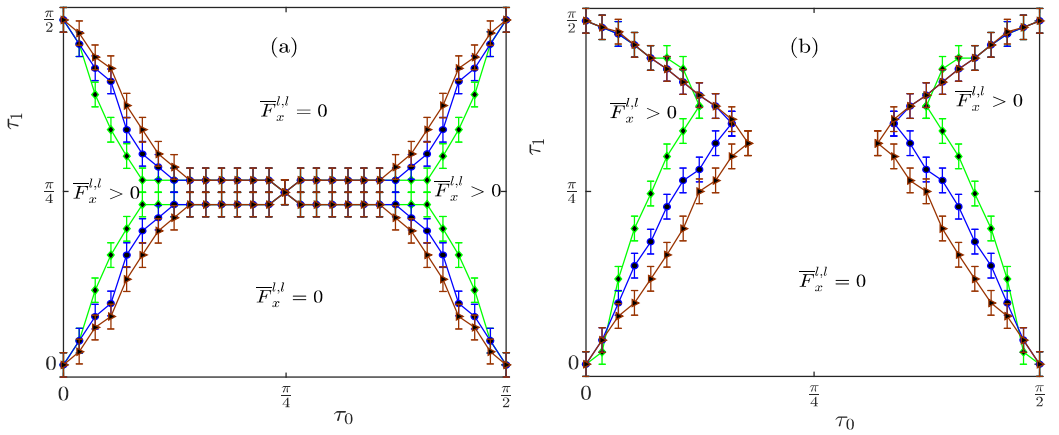


Fig. 2.7 Regions with $\overline{F}_x^{l,l}(T) > 0$ and $\overline{F}_x^{l,l}(T) = 0$ in the $\tau_0$ and $\tau_1$ parameter space with $T = 10^4$, for the (a)closed and (b) open chain Floquet systems of system size N=6(Green), 8(Blue) and 10(Brown). As increasing system size, critical lines of both (a) and (b) tend towards diagonal critical lines. Hence, this suggests that the phase structure of the system would contain two ferromagnetic regions (where $\overline{F}_x^{l,l} > 0$) and two paramagnetic regions (where $\overline{F}_x^{l,l} = 0$).

the second kick ($n = 2$) will be

$$\begin{aligned} F_x^{l,l}(2) &= \frac{1}{64}\Big[\cos(4\tau_0)(21 - 4\cos(4\tau_1) - 17\cos(8\tau_1)) \\ &+ \cos(12\tau_0)(-5 + 4\cos(4\tau_1) + \cos(8\tau_1)) \\ &+ 2(5 - 12\cos(4\tau_1) + 7\cos(8\tau_1) + \cos(8\tau_0) \\ &\times (19 + 12\cos(4\tau_1) + \cos(8\tau_1)))\Big] \end{aligned}$$

Again we see that $F_x^{l,l}(1)$ and $F_x^{l,l}(2)$ have $\tau_0$ and $\tau_1$ are in a multiple of $4k$, where $k$ is the integer. Therefore, LMOTOC will be same for (1) $\tau_0$ and $\frac{\pi}{2} - \tau_0$, and (2) $\tau_1$ and $\frac{\pi}{2} - \tau_1$ and symmetric about $\tau_0 = \frac{\pi}{4}$ and $\tau_1 = \frac{\pi}{4}$ in the closed chain system.

In the closed chain Floquet system, the tips of the regions with $\overline{F}_x^{l,l} = 0$ can be seen to be moving closer to each other along the line $\tau_1 = \frac{\pi}{4}$, with increasing the system size [Fig. 2.7(a)]. In the open boundary condition, the tips, which start out in the upper half

of the parameter space, also move downwards towards the point $(\frac{\pi}{4}, \frac{\pi}{4})$ with increasing system size [Fig. 2.7(b)].

### 2.7.1 Critical line with system size

Behavior of increasing the tips with increasing system size in closed chain case can be understood by the finite size effect analysis, which is given as [122]

$$|\tau_{0c}(N) - \tau_{0c}(\infty)| \propto N^{-1/\nu}, \tag{2.13}$$

where $\tau_{0c}(N)(\tau_{0c}(\infty))$ is the location of the critical point on the horizontal axis of the phase structure of the finite system size [Fig. 2.7(a)] (infinite system size [Fig. 2.1]). $\nu$ is the transverse field exponent defined as the reciprocal of the slope of the straight line drawn from $|\tau_{0c}(N) - \tau_{0c}(\infty)|$ *vs* system size $(N)$ (log-log plot). As evident from Fig. 2.8, increasing the system size $N$ leads to closing the gap between $\tau_{0c}(N)$ and $\tau_{0c}(\infty)$. In the thermodynamic limit, we expect the tips to meet at the center, giving the diagonal lines as shown in Fig. 2.1. A similar argument holds true for the open chain case. Hence, the time-averaged LMOTOC $[\overline{F}_x^{l,l}(T)]$ for large $T$ and $N \to \infty$ can be used as an order parameter to distinguish the phases of a driven transverse field Floquet Ising model. It must be noted that the time-averaged LMOTOC does not distinguish between the ferromagnetic and the $\pi$ ferromagnetic phase or the paramagnetic and the $0\pi$ paramagnetic phase. However, these distinct phases can be identified by observing the combined eigenvalues at the edges of the phase structures of the unitary operator which is defined in Eq. (2.1) and the parity operator ($P = \prod_l \sigma_l^z$) [106, 109]. Considering the operators $\hat{U}$ and $\hat{P}$ have eigenvalues $u$ and $p$, respectively, the different phases can be distinguished by observing the eigenvalues along the outer edges of the phase diagram. The eigenvalues have protected multiplets of the form: $(u, p)$ in the paramagnetic, $[(u, p), (u, -p), (-u, p), (-u, -p)]$ in

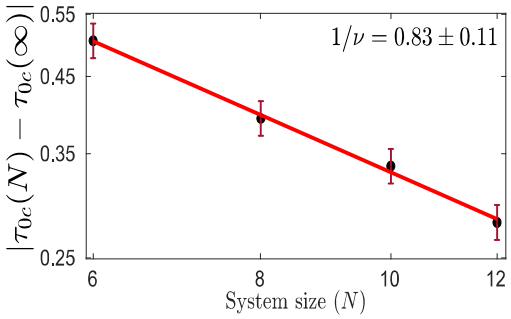


Fig. 2.8 Plot of the difference between finite size critical point and the infinite size critical point ($|\tau_{0c}(N) - \tau_{0c}(\infty)|$) of the phase structure of the periodic Floquet system as the function of system size (log-log plot). Black points are data points, and the red dashed line is the best fit yielding the slope $1/\nu = 0.8314 \pm 0.1122$.

the $0\pi$ paramagnetic, $[(u,p),(u,-p)]$ in the ferromagnetic and $[(u,p),(-u,-p)]$ in the $\pi$ ferromagnetic regions.

## 2.8 Phase structure by frequencies of oscillations

The frequencies of oscillations of the LMOTOC also provide a signature of the phase transitions. Here, the dominant frequencies have been numerically determined by taking the argument maxima of the discrete Fourier transforms of the deviation of the LMOTOC from its mean value ($F_x(n) - \overline{F}_x(T)$). Mathematically, it can be defined as:

$$\mathscr{F}(\nu) = \frac{1}{T}\sum_{n=1}^{T}[F_x(n) - \overline{F}_x(T)]e^{-i\frac{2\pi}{T}\nu n} \tag{2.14}$$

A heatmap of the dominant frequencies of $\mathscr{F}(\nu)$ in the logarithmic scale is shown in Fig. 2.9 for $N = 10$ in the closed and open boundary conditions. These plots show that the dominant frequencies logarithmically drop close to the critical lines and at the edges. Comparing Fig. 2.9 and Fig. 2.7, we observe that heatmap displays indications of the phase transition in the Floquet Ising system.

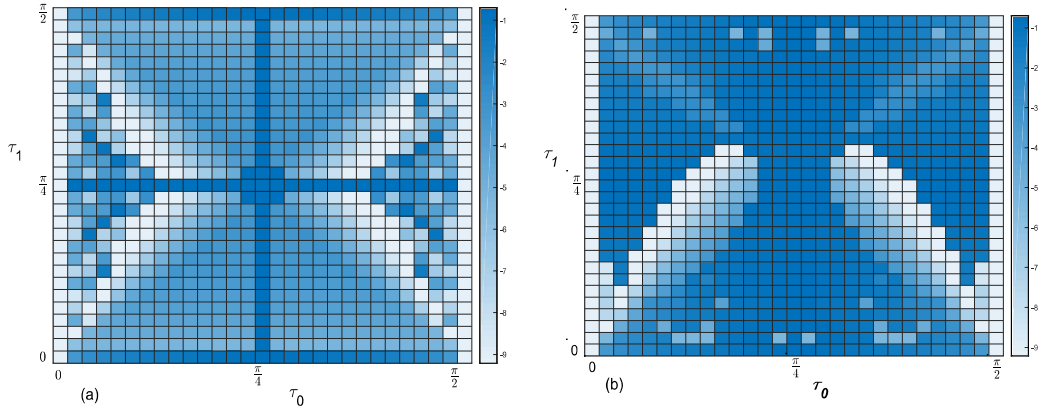


Fig. 2.9 Heat map of the logarithmic dominant frequencies of $F(n) - \overline{F}_x(T)$ in the discretized $\tau_0$-$\tau_1$ parameter space for the (Left) closed and (Right) open Floquet system of system size $N = 10$ and with $T = 10^4$. The heat map shows logarithmically small values close to the transition lines shown in Fig. 2.7.

## 2.9 Conclusion

We calculated the exact analytical expression for TMOTOC as a function of $\tau_0$ and $\tau_1$. With the help of the analytical formulation, we calculated the speed of commutator growth for the TMOTOC and compared it with those of the LMOTOC. We also analyzed the revival of the initial state and found that the TMOTOC revived back within a finite time while LMOTOC did not. Further, we study the phase structure of the traverse field Floquet system given by Eq. (2.1) using numerical calculation of LMOTOC. We use LMOTOC defined in equation Eq. (2.4) to distinguish between the paramagnetic and ferromagnetic phases of the chosen Floquet system. Ferromagnetic and $\pi$ ferromagnetic phase or paramagnetic and $0\pi$ paramagnetic phases are distinguished by the combined eigenvalues of unitary operator $\hat{U}$ and parity operator $\hat{P}$ along the edges of the phase structures. We numerically find the time averaged LMOTOC $[\overline{F}_x^{l,l}(T)]$ for the system sizes up to $N = 10$ and plot the regions of the parameter space that have $\overline{F}_x^{l,l}(T) = 0$ and $\overline{F}_x^{l,l}(T) > 0$ for $T = 10^4$. We observe that the plot showing the critical lines of phase transition for $N \to \infty$ tends to the expected plot Fig. 2.1. In the limit $N \to \infty$, the regions with $\overline{F}_x^{l,l}(T) > 0$ for large $T$ are ferromagnetic

and those with $\overline{F}_x^{l,l}(T) = 0$ for large $T$ are paramagnetic.

OTOCs can be experimentally calculated [101], and Floquet systems can be experimentally realized [123]. Our study outlines the analytical calculation of the TMOTOC, its behavior with the separation between the observables, and how LMOTOC can be a useful tool to distinguish the phases of a Floquet system.

In the next chapter, we will discuss three different regimes such as characteristic, dynamic, and saturation regions of LMOTOC and TMOTOC in both integrable and nonintegrable Ising spin Floquet systems.